



HAL
open science

FEM simulation on elastic parameters of porous silicon with different pore shapes

Xiaoyue Gong, Julien Bustillo, Laurianne Blanc, Gaël Gautier

► **To cite this version:**

Xiaoyue Gong, Julien Bustillo, Laurianne Blanc, Gaël Gautier. FEM simulation on elastic parameters of porous silicon with different pore shapes. *International Journal of Solids and Structures*, 2020, 190, pp.238-243. 10.1016/j.ijsolstr.2019.11.001 . hal-03211325

HAL Id: hal-03211325

<https://hal.science/hal-03211325>

Submitted on 7 Mar 2022

HAL is a multi-disciplinary open access archive for the deposit and dissemination of scientific research documents, whether they are published or not. The documents may come from teaching and research institutions in France or abroad, or from public or private research centers.

L'archive ouverte pluridisciplinaire **HAL**, est destinée au dépôt et à la diffusion de documents scientifiques de niveau recherche, publiés ou non, émanant des établissements d'enseignement et de recherche français ou étrangers, des laboratoires publics ou privés.



Distributed under a Creative Commons Attribution - NonCommercial 4.0 International License

FEM simulation on elastic parameters of porous silicon with different pore shapes

Xiaoyue Gong · Julien Bustillo · Laurianne Blanc · Gaël Gautier

Received: date / Accepted: date

Abstract Porous silicon (PSi) seems to be a promising material for acoustic transducers due to its manufacturing ease and high abilities. Yet, the investigation on wave propagation in this porous material is required to enhance the sensitivity. According to Biot's theory, wave propagation is governed by the porous matrix moduli (*i.e.* Young's modulus, bulk modulus, and shear modulus). These parameters as well as Poisson ratios are difficult to measure and are often estimated using ultrasonic measurements. In this paper, the elastic parameters of porous silicon skeleton varying with porosity are investigated using FEM simulations. The silicon substrate from which the PSi is formed has a (100) crystallographic orientation and the pores are cylinder-like. Six pore shapes were designed in order to investigate the influence of pore morphology on elastic parameters. These shapes are chosen according to the pore geometries obtained by electrochemical etching and designed as orthotropic structures. The results show that the morphology of the pores has a significant influence on the elastic moduli, therefore, should be taken into consideration in further research. The simulation results are in good agreement with the experimental data reported in literature for Young's modulus. Moreover, the power-law fittings of Young's moduli and the shear moduli as functions of porosity are proposed and the fitting errors are discussed.

Keywords porous silicon · elastic moduli · orthotropic · pore morphology · FEM

J. BUSTILLO
GREMAN UMR 7347 CNRS
INSA Centre Val de Loire, 3 Rue de la Chocolaterie, 41000 Blois
Université de Tours, France
Tel.: +33-06-50-41-31-27
E-mail: julien.bustillo@insa-cvl.fr

1 Introduction

As an artificial material whose morphology can easily be controlled during the manufacturing process, porous Silicon (PSi) seems to be a very promising material in many areas, *e.g.* drug delivery [1], anodes [2], dye-sensitized solar cells [3], micro-fuel cells [4], *etc.* PSi could also be compatible with acoustic transducers [5] with cleanroom manufacturing, and can be integrated into lab-on-chips systems. Yet, to optimize the performance of PSi in the acoustic applications, the wave propagation and the factors that will affect this propagation in this material needs to be accurately characterized. For this purpose according to Biot's theory [6,7], a good knowledge of the elastic parameters (including elastic moduli and the Poisson ratio) of PSi is required.

The optical, electrical and thermal properties of PSi have been widely studied [8,9] due to their numerous application fields. Similarly, the elastic properties of PSi have also been studied by several researchers. For example, using X-Ray Diffraction, K. Barla *et al.* [10, 11] showed that the lattice constant of the porous layer increases according to the porosity ϕ (the volumetric ratio of pores to the bulk PSi). Young's modulus was directly related to lattice constants and thus, to the pore morphology. Da Fonseca *et al.* [12,13] used acoustic microscopy to investigate the acoustic properties of PSi manufactured from p+-type (100) crystalline silicon wafer. He described the longitudinal and shear wave velocities, V_L and V_S , as empirical functions of porosity as $V_{L/S} = V_{L0/S0}(1 - \phi)^n$, where subscript '0' refers to the velocity in crystalline silicon and n is a fitting parameter depending on pore shape. Measurements have shown a good agreement with theory using Da Fonseca formulas [14, 15]. Using transmission spectroscopy, G. N. Aliev *et al.* [16] derived a semi-empirical relation of wave velocity and porosity which is the same as Fonseca's fitting formula. They assumed that the Poisson ratio of PSi (ν_p) is independent of ϕ . Based on this as-

sumption, Martini *et al.* [17] have studied the mechanical properties of sintered mesoporous silicon using Finite Element Methods (FEM). Thus, they modeled PSi using randomly distributed spherical pores and concluded that the properties of the sintered PSi are in good agreement with experiments. D. Bellet *et al.* [18] applied nano-indentation technique to the investigation of Young's modulus of PSi with porosity ranging from 36% to 90% and showed that the doping level has an influence on PSi Young's modulus. Moreover, they pointed out that the main difference between p+ and p-type PSi is the pore morphology. By taking PSi Poisson ratio as a constant ($\nu_p = 0.10$), Bellet concluded that the p+-type-(100) oriented PSi Young's modulus follows a power-law function: $E_p = A(1 - \phi)^2$, where $A = 120 \text{ GPa}$. By using a discrete homogenization approach, Magoaric and Danesny [19] treated PSi as a cubic material and gave a similar function as Bellet. C. Populaire *et al.* [20] proposed a new function for Young's modulus as: $E_p = E_0(1 - \phi)^2$, where E_0 is the Young's modulus of crystalline silicon.

The works above gave explanations on the microscopic mechanics of elastic parameters of PSi and they all mentioned that pore structure is one of the key factors for estimating the elastic properties of PSi. But their discussions are limited by their assumptions, such as constant Poisson ratio. Moreover, the anisotropic property of PSi has not been mentioned. While, the discussion of porous materials' anisotropic properties has a theoretical basis presented in [21], where the equations for general cases of porous medium are presented. In particular, the isotropic case is detailed and the case of orthotropic and transverse isotropic are mentioned. Therefore, it is necessary to investigate in detail the anisotropic properties of our material. To this end, an investigation of the influence on its elastic properties corrected to pore structure is proposed. Considering the influence of these factors cannot be easily studied or quantified by experiments, FEM simulations are proposed in this article.

Thus, the following part of the paper presents the theoretical background used for elastic parameters determination is presented. Then, the numerical simulations performed on six different shapes that correspond to common pore geometries are detailed. Finally, the results of simulated elastic parameters of our orthotropic PSi models are presented and discussed.

2 Theoretical background

The microscopic analysis of an elastic wave propagating in a solid begins by the definition of stress-strain relation. The Hooke's law formulates this relation as:

$$\sigma = C \cdot \mathbf{e} \quad (1)$$

where σ is the stress tensor (either compression or an extension) applied to a given medium and \mathbf{e} is the resultant strain tensor; C is the stiffness tensor. In the case of crystals, the tensors σ and \mathbf{e} have orders of two, while C is a four-ordered tensor. The number of independent components in C depends on the symmetry of the crystal (up to 21 for triclinic). For an orthotropic structure which has three mutually-orthogonal twofold symmetry axes, its stiffness tensor has nine independent parameters that can be written in the matrix form as:

$$C = \begin{bmatrix} c_{11} & c_{12} & c_{13} & 0 & 0 & 0 \\ c_{12} & c_{22} & c_{23} & 0 & 0 & 0 \\ c_{13} & c_{23} & c_{33} & 0 & 0 & 0 \\ 0 & 0 & 0 & c_{44} & 0 & 0 \\ 0 & 0 & 0 & 0 & c_{55} & 0 \\ 0 & 0 & 0 & 0 & 0 & c_{66} \end{bmatrix} \quad (2)$$

In the case of a material having cubic symmetry, such as crystalline silicon, only 3 components are independent in its C ($c_{12} = c_{13} = c_{23}$, $c_{11} = c_{22} = c_{33}$ and $c_{44} = c_{55} = c_{66}$). Using formulas (1) and (2), the elastic parameters of crystalline silicon can be deduced from its stiffness tensor [16][22] as:

$$\begin{aligned} E_0 &= \frac{1}{2} \frac{(c_{11} - c_{12})(c_{11} + 2c_{12})}{c_{11} + c_{12}} \\ \nu_0 &= \frac{c_{12}}{c_{11} + c_{12}} \\ G_0 &= c_{44} \\ K_0 &= \frac{c_{11} + 2c_{12}}{3} \end{aligned} \quad (3)$$

where E_0 is the Young's modulus, ν_0 the Poisson ratio, G_0 the shear modulus and K_0 the bulk modulus. Since it is orthotropic material, its elastic parameters vary with directions. Therefore, to be specified, the subscript "0" stands for the principle direction of bulk solids, without any pores inside.

Hooke's Law can also be rewritten as a strain-stress relationship:

$$\mathbf{e} = S \cdot \sigma \quad (4)$$

where S is the compliance tensor which equals to the inverse of the stiffness tensor C . This relationship is useful to estimate the elastic parameters of an orthotropic medium as it is directly related to the Young's modulus E_i , Shear modulus, G_{ij} and Poisson ratio ν_{ij} in each direction as shown in formula (5). Here, the coordinates are set to be parallel to the principle directions of the silicon crystal, *i.e.* the x-axis aligns to [100], y-axis to

[010], and z-axis to [001].

$$\begin{bmatrix} e_x \\ e_y \\ e_z \\ \gamma_{yz} \\ \gamma_{zx} \\ \gamma_{xy} \end{bmatrix} = \begin{bmatrix} \frac{1}{E_x} & -\frac{\nu_{yx}}{E_y} & -\frac{\nu_{zx}}{E_z} & 0 & 0 & 0 \\ -\frac{\nu_{xy}}{E_x} & \frac{1}{E_y} & -\frac{\nu_{zy}}{E_z} & 0 & 0 & 0 \\ -\frac{\nu_{xz}}{E_x} & -\frac{\nu_{yz}}{E_y} & \frac{1}{E_z} & 0 & 0 & 0 \\ 0 & 0 & 0 & \frac{1}{G_{yz}} & 0 & 0 \\ 0 & 0 & 0 & 0 & \frac{1}{G_{zx}} & 0 \\ 0 & 0 & 0 & 0 & 0 & \frac{1}{G_{xy}} \end{bmatrix} \cdot \begin{bmatrix} \sigma_x \\ \sigma_y \\ \sigma_z \\ \tau_{yz} \\ \tau_{zx} \\ \tau_{xy} \end{bmatrix} \quad (5)$$

It is seen that these elastic parameters relate the stress to the resulted strain. As a result, the elastic parameters can be obtained by applying different kinds of stress loads and observing the associated strains. As an example, by applying a normal stress (tension or compression) σ_i on ik - surface of porous medium, with the lateral surfaces being free, we obtain relations $e_i = \sigma_i/E_i$, $e_j = -(\sigma_i\nu_{ij})/E_i$, and $e_k = -(\sigma_i\nu_{ik})/E_i$ from formula (5). By inverting these relations, the elastic parameters are deduced:

$$\begin{aligned} E_i &= \sigma_i/e_i \\ \nu_{ij} &= -e_j/e_i \\ G_{ij} &= \tau_{ij}/\gamma_{ij} \end{aligned} \quad (6)$$

Considering the axial symmetry of the pores, we also have the following relations: $E_y = E_z$; $\nu_{xy} = \nu_{xz}$, $\nu_{yx} = \nu_{zx}$, $\nu_{yz} = \nu_{zy}$, thus the number of independent elastic parameters for an orthotropic material is reduced.

By applying a hydrostatic pressure on the surface of the medium, *i.e.* $\sigma_x = \sigma_y = \sigma_z = p$, and shear stress $\tau_x = \tau_y = \tau_z = 0$, then $e_x = (\frac{1}{E_x} - \frac{\nu_{yx}}{E_y} - \frac{\nu_{zx}}{E_z})p$, $e_y = (\frac{1}{E_x} - \frac{\nu_{yx}}{E_y} - \frac{\nu_{zy}}{E_z})p$, $e_z = (\frac{1}{E_x} - \frac{\nu_{xz}}{E_x} - \frac{\nu_{yz}}{E_y})p$. Finally, the bulk modulus for PSi K_b is deduced by the relation:

$$K_b = \frac{p}{e_x + e_y + e_z} \quad (7)$$

which means that the bulk modulus is computed using the hydrostatic pressure divided by the resultant volume decrement. According to the formula (6) and (7), it is convenient to use FEM simulations to compute the elastic parameters.

3 Numerical simulations

In this paper, we will consider only the PSi obtained by electrochemical etching on silicon wafer[23]. According to the morphology characterization of PSi through SEM (scanning electron microscope) imaging, PSi is treated as orthotropic porous material. It is considered that the PSi is etched from a (100) oriented silicon wafer, and the geometric model used for simulations is with straight and periodically distributed pores oriented to the x-coordinate. The values of the stiffness constants (the independent components of C) for a [100] oriented pure silicon crystal are shown in Table 1 [24].

Table 1 Values of stiffness constants (in GPa) for Silicon at room temperature

c_{11}	c_{12}	c_{44}
165.6	63.9	79.5

Table 2 Values of elastic parameters for bulk Silicon at room temperature

E_0	ν_0	G_0	K_0
130GPa	0.28	79.5GPa	97.8GPa

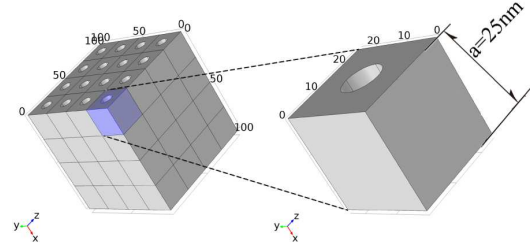


Fig. 1 The RVE of PSi sample with cylindrical pores parameter a represents the spatial period.

By using formulas (3) and the values in Table 1, the corresponding elastic parameters for bulk silicon are then calculated and presented in Table 2.

In order to lower the computational cost, the pores are set to be uniform and axisymmetric, thus, a cubic sample with only one pore in its middle is good enough to be a representative volume element (RVE). The spatial period of the cubic RVE is set as $a = 25nm$, as shown in Fig. 1. It is worth mentioning that this spatial period does not affect the simulation results for elastic parameters, and it is defined here only for FEM computations. The inside of the pore is empty, *i.e.*, without any fluids or particles. The remaining solid part, or the skeleton, of the cube is pure silicon.

Thanks to the symmetries, periodic boundary conditions are set to further decrease the computation cost. Fig. 2 shows an example set of boundary conditions for the simulation on Young's modulus along x-axis where an extension stress parallel to the x-direction is loaded on the yz- surface of the RVE. After FEM computing, the displacement vector $\mathbf{u} = (u, v, w)$ and the strain tensor $\mathbf{\epsilon}$ of the RVE are obtained. Fig. 3 illustrates the computation result for displacement under the boundary conditions described in Fig. 2. Thus, based on formula (6), E_i , ν_{ji} and G_{ji} can be obtained. According to stress-strain relation (5), components of the compliance tensor of PSi (s_{ij}) is then calculated, as well as the stiffness tensor C (by inverting S).

In fact, pores in PSi are not always as perfect as cylinders, but present different morphologies depending on the etching conditions and substrate properties like doping type and level, crystalline orientation, *etc.* [25]. It has been shown that pores etched at low cur-

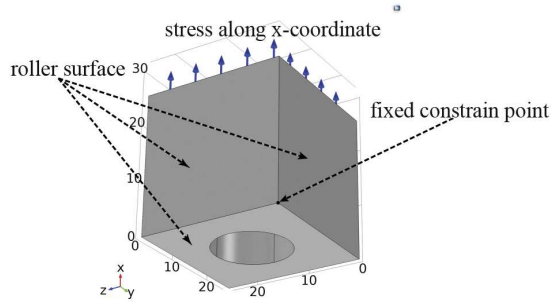


Fig. 2 Description of boundary conditions for computing Young's modulus E_x

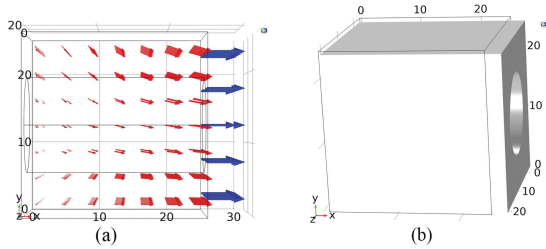


Fig. 3 (a) The normal stress loaded on x-direction (blue arrows) and the displacement field (red arrows); (b) Deformation of PSi

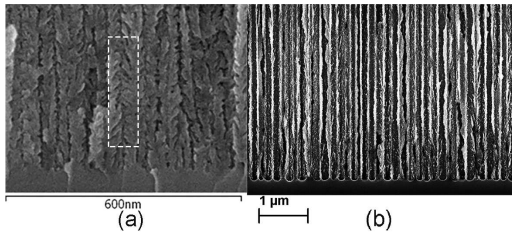


Fig. 4 Cross sections of typical pore shapes via SEM image (a) PSi exhibits a branched morphology [27]. (b) PSi with bigger and cylindrical pores (image comes from lab. GREMAN)

rent density generally have lower porosity and exhibit branched morphology [26], like in Fig. 4(a) [27]. On the contrary, high current density generally leads to bigger pores, with a cylindrical morphology, like in Fig. 4(b) (image comes from lab. GREMAN).

Thus, to extend the study range and obtain reliable results, different kinds of pore morphology are investigated. Firstly, in addition with the cylindrical pore in Fig. (1), four other typical pore shapes have been designed (shown in Fig. 5 according to achievable PSi morphology, and they are respectively named as: cylindrical, sin-shaped, two-radius, varying-radius and branched models. To be specific, the sin-shaped model shows small radius variations of the pores and the shape of the wall does not change with the increase of pore size; the two-radius model has two different radii of pores with a ratio of 1:1.5; the varying-radius model has great radius variation on the pore wall and this variations increases with the growth of pore size; the branched model has several side branches symmetrically distributed along the main cylindrical pore. In addition, the studied crystalline orientation is $\langle 100 \rangle$ and the pore direc-

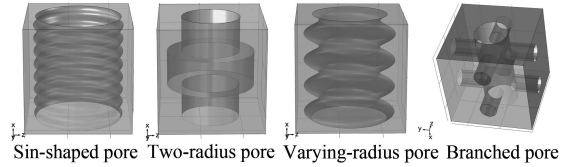


Fig. 5 Different morphological models implemented in the FEM simulation.

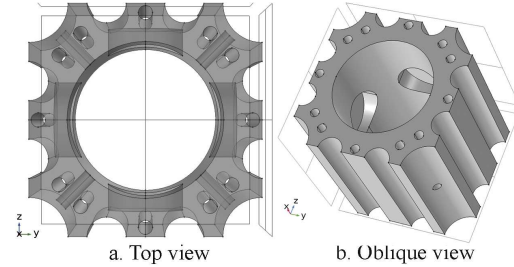


Fig. 6 Hybrid model (one main cylindrical pore with both side branches and secondary pores).

tion is parallel to X-axis. Multiple porosities are obtained by changing the size of the pores. By using these morphological models, the influence of pore shapes on the elastic parameters can be studied. It is worth noting that, the computed results for the elastic parameters here are actually for the RVEs, therefore, they are regarded as the effective values of the PSi being an elastic material.

In addition, considering the pore morphologies given in Fig. 5, the porosity is limited to 63%. To reach higher porosities, a hybrid model with secondary pores and branches is proposed accordingly. The designed example in Fig. (6) is for a porosity of 60%. It is close to a branched model at lower porosity, while with the increase of porosity, it becomes more like a combination of cylinders with different radii. The porosity of this model can reach up to 89%.

4 Results and discussions

The simulated results are presented firstly by comparing with data from the literature to show the reliability. Then, by plotting the elastic moduli and fitting them as power laws of porosity, the differences in the elastic moduli between the six models are presented and analyzed.

Fig. 7 is the comparison between our FEM simulation results for E_y of branched and hybrid model and Young's modulus measured by other researchers with different approaches. At both low and high porosity range, it seems that our FEM results have higher consistency with the results of D. Bellet *et al.* [18] using nanoindentation technique, as well as with the numerical results of Magoariec *et al.* using discrete homogenization approach [19]. The discrepancy appearing between our FEM method and the discrete homog-

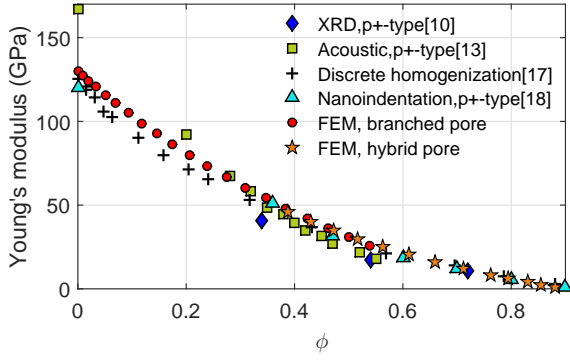


Fig. 7 Comparison of Young's modulus of PSi obtained from FEM simulations with data given by other research methods (experimental and simulation based)

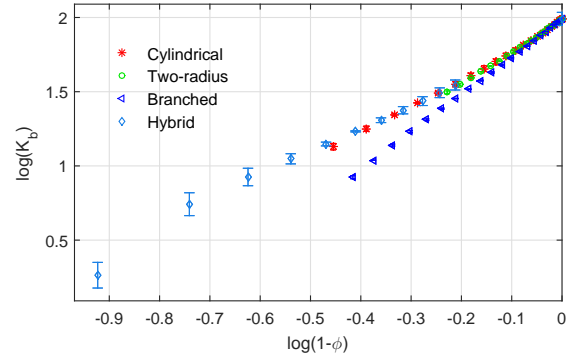


Fig. 9 Bulk modulus of PSi with different pore shapes

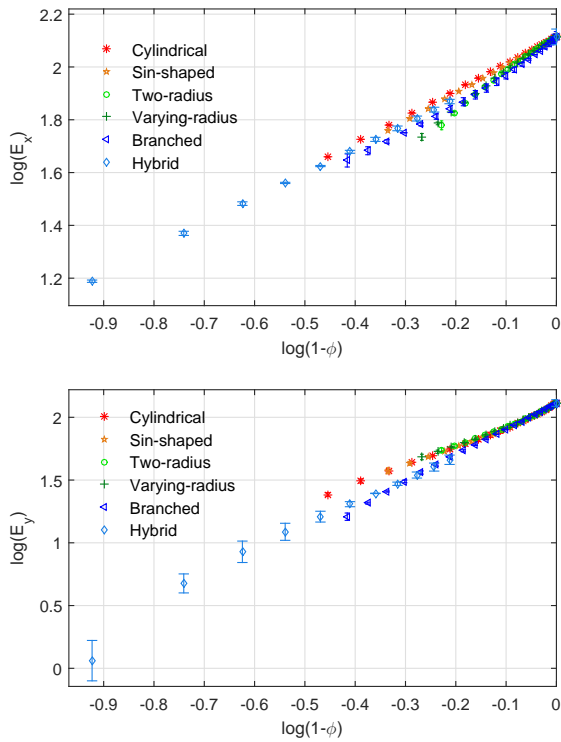


Fig. 8 Young's modulus of PSi with different pore shapes (It should be noted that because of the symmetry of our geometrical models, E_z is identical to E_y .)

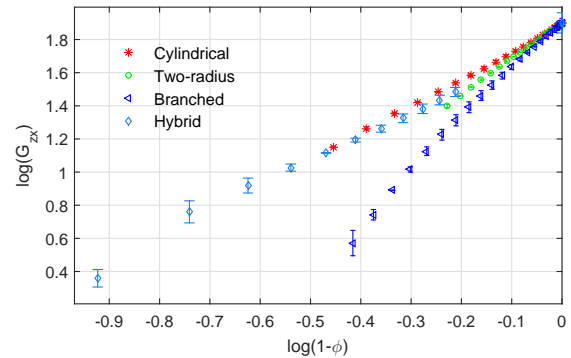
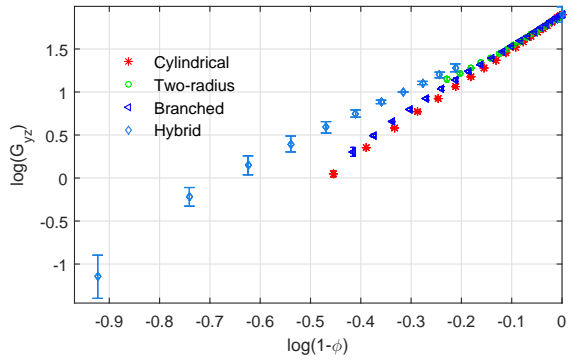
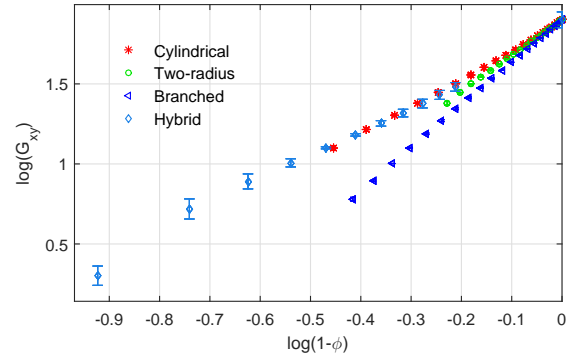


Fig. 10 Shear modulus of PSi with different pore shapes

ization method at lower porosity indicates that, the symmetry of the PSi model can influence on its elastic moduli. Therefore, the anisotropic property of the skeleton should be taken into consideration, especially at lower porosity ($< 40\%$).

The FEM simulation results for Young's modulus, bulk modulus, and shear modulus are respectively presented in Fig. 8, Fig. 9 and Fig. 10. The influence of the pore shapes and the porosity on the elastic properties of PSi therefore can be observed from the variations and divergences.

From Fig. 8 to 10 it is seen that the evolution of elastic moduli (*i.e.* Young's modulus, bulk modulus

and shear modulus) as a function of porosity clearly have dependence on the pore geometry. While it is also clear that the influence of pore shapes is different on each elastic modulus, some similarities between these pore models are observed. For example, elastic parameters with the cylindrical and sin-shaped geometries are roughly equal, so are the two-radius and varied-radius geometries. In fact, it is because that the pore radius does not drastically change between sin-shaped and cylindrical geometry, whereas the two-radius pore and varied-radius geometry have huge variations of the radius on the x -axis direction. Therefore, the sin-shaped and varying-radius models are not shown in Fig 9 and 10. Nevertheless, the bulk modulus is very similar for all of the geometries except for the branched one. In conclusion, it can be pointed out that, some small variation on the pore wall is negligible, but branches significantly differ all the elastic parameters of PSi.

Fitting functions of Young's modulus E and shear modulus G of PSi have been proposed by Martini, *et al.* [17] as a power law of the porosity defined by:

$$\begin{aligned} E &= E'_0(1 - \phi)^m \\ G &= G'_0(1 - \phi)^h \end{aligned} \quad (8)$$

where E'_0 and G'_0 are scale factors which normally equal respectively to the Young's modulus and shear modulus of crystalline silicon (presented in equation (3) and Table 2). m and h are the fitting numbers.

Using these formulations, m and h have been fitted from numerical values of the elastic parameters. They are given in Table 3 for the Young moduli and shear moduli. The fitting errors err_i are also calculated based on formula (9) to indicate the precision of the fitting, where y_i is the simulated result, y'_i is the fitting result and i stands for the position of the data. err_i are presented as error bars in Fig. 8 to Fig. 10, from which it is observed that the power-law fittings have good agreement with simulated results at lower porosity for the cylindrical model, two-radius model and branched model, but the error becomes higher for higher porosity, like for the hybrid model. Thus, the fittings are not reliable enough for this range of porosity. Moreover, it should be mentioned that the scale factors here are slightly different from E_0 or G_0 in Table 2. The power-law fittings are just rough estimations of the relations between the elastic moduli and porosity.

$$err_i = y_i - y'_i \quad (9)$$

In addition, the fitting numbers m and h for the hybrid model listed in Table 3 show great difference with the others. This is because they deviate greatly from a simple power law and have scale factors greatly distinguished from E_0 and G_0 . This is also observed intuitively in Fig. 8 to 10. While they have different continuity with the results of the other pore models, for

Table 3 Fitting parameters of power law for Young's and shear moduli

shape	m		h		
	(E_x)	(E_y)	(G_{xy})	(G_{yz})	(G_{zx})
cylindrical	1.00	1.58	1.76	3.99	1.64
sin-shaped	1.05	1.62	1.85	3.89	1.72
two-radius	1.43	1.66	2.24	3.36	2.16
varying-radius	1.40	1.62	2.25	3.43	2.14
branched	1.14	2.11	2.67	3.74	3.08
hybrid	0.97	2.05	1.57	3.07	1.49

example, in terms of E_y , the hybrid model succeeds the trend of the branched model, but for G_{xy} , it behaves more like an extension of the cylindrical model.

Values of fitting number m and h for the first five shape models (from cylindrical to branched model) are close to the values given by Roberto Martini, except for G_{yz} . The divergence comes from the model differences, and mainly because the Poisson ratio of PSi was considered as a constant in [17]. As shown in our study, the Poisson ratio not only changes with porosity but also with pore shapes and orientations. It can also be observed that the values for cylindrical and sin-shaped models are close, whereas the two-radius and the varying-radius models are close. Thus, they can be grouped into two families.

5 Conclusion

In this paper, the influence of the pore shape on elastic parameters with different porosities has been successfully observed by studying several typical morphological models of PSi. Results have been obtained by FEM simulations. From the analysis of the results and the comparison with experimental data from the literature, it can be concluded that when the porosity increases, the PSi elastic parameters decrease following some patterns. In addition, the pore shape has a significant effect on those patterns, especially for the branched pore model. But there still exist some simplifications on pore shape modeling, *i.e.*, according to the FEM results for cylindrical and sin-shaped pore, when there are only small variations on the pore wall, its geometrical model can be simplified as cylinders; whereas when the variations of the pore wall is too huge to be ignored, like varying-radius pore given in this paper, it may be regarded as two-radius model; nevertheless, when there are branches on sides of the main pore, they can not be disregarded or simplified. These results can be very useful when modeling on PSi.

In further work, coupling between solid and fluid phases will be investigated in order to be included in Biot theory. Then, wave propagation in a real porous silicon layer could be simulated or calculated according to its real geometrical parameters. It is worth men-

tioning that when talking about the wave velocity of PSi, the propagation direction should be taken into consideration, since PSi can strongly behave anisotropically, especially in low porosity samples (< 40%). Therefore, wave equations for anisotropic porous materials will be presented and solved in the following work.

Conflict of Interest

The authors declare that they have no conflict of interest.

References

- Emily J. Anglin, Lingyun Cheng, William R. Freeman, and Michael J. Sailor. Porous silicon in drug delivery devices and materials. *Advanced Drug Delivery Reviews*, 60(11):1266–1277, 2008.
- Zhenda Lu, Nian Liu, Hyun Wook Lee, Jie Zhao, Weiyang Li, Yuzhang Li, and Yi Cui. Nonfilling Carbon Coating of Porous Silicon Micrometer-Sized Particles for High-Performance lithium battery anodes. *ACS Nano*, 9(3):2540–2547, 2015.
- Jan Hendrik Petermann, Dimitri Zielke, Jan Schmidt, Felix Haase, Enrique Garralaga Rojas, and Rolf Brendel. 19%-efficient and 43 μm -thick crystalline si solar cell from layer transfer using porous silicon. *Progress in Photovoltaics: Research and Applications*, 20(1):1–5, 2012.
- Gaël Gautier and Sebastien Kouassi. Integration of porous silicon in microfuel cells: a review. *International Journal of Energy Research*, 39(1):1–25, jan 2015.
- Julie Lascaud, C. Compère, D. Certon, T. Defforge, D. Alquier, and Gaël Gautier. Integration of porous silicon on the rear side of capacitive micromachined ultrasonic transducers. In *proceeding*, pages 237–238, Montpellier, 2018. PSST conference.
- Maurice Anthony Biot. Theory of Propagation of Elastic Waves in a Fluid-Saturated Porous Solid. I. Low Frequency Range. *The Journal of the Acoustical Society of America*, 28(2):168–178, 1956.
- Maurice Anthony Biot. Theory of Propagation of Elastic Waves in Fluid-Saturated Porous Solid. II. Higher frequency range. *The Journal of the Acoustical Society of America*, 28(2):179–191, 1956.
- Leigh Canham. *Handbook of Porous Silicon*. Springer, 2014 edition, 2014.
- Mansour Aouassa, Latifa Hassayoun, Luc Favre, Antoine Ronda, and Isabelle Berbezier. Optimization of structural and optical properties of nanoporous silicon substrate for thin layer transfer application. *Journal of Materials Science: Materials in Electronics*, 30(3):2585–2591, 2019.
- Kathy Barla, Roland Hérino, Guillermo Bomchil, Jean Claude Pfister, and Andreas K. Freund. Determination of lattice parameter and elastic properties of porous silicon by X-ray diffraction. *Journal of Crystal Growth*, 68(3):727–732, 1984.
- Reza S. Dariani and M. Nazari. Comparison of stress, strain, and elastic properties for porous silicon layers supported by substrate and corresponding membranes. *Journal of Molecular Structure*, 1119:308–313, 2016.
- R. J. M Da Fonseca, J. M. Saurel, and G. Despau. Elastic characterization of porous silicon by acoustic microscopy. *Superlattices and Microstructures*, (July):21–23, 1994.
- Raul José da Silva Camara Mauricio da Fonseca. *Microcaractérisation élastique de matériaux poreux par signature acoustique*. PhD thesis, Université des sciences et techniques de Montpellier, 1995. Thèse de doctorat dirigée par Attal, Jacques Électronique, optronique et systèmes Montpellier 2 1995.
- Julien Bustillo, Jérôme Fortineau, Gaël Gautier, and Marc Lethiecq. Ultrasonic characterization of electrochemically etched porous silicon. *Japanese Journal of Applied Physics*, 53(6):1–4, 2014.
- Julien Bustillo, Jérôme Fortineau, Gaël Gautier, and Marc Lethiecq. Ultrasonic characterization of porous silicon using a genetic algorithm to solve the inverse problem. *NDT and E International*, 62:93–98, 2014.
- Gazi N. Aliev, Bernhard Goller, and Paul A. Snow. Elastic properties of porous silicon studied by acoustic transmission spectroscopy. *Journal of Applied Physics*, 110(4):1–8, 2011.
- Roberto Martini, Valerie Depauw, Mario Gonzalez, Kris Vanstreels, Kris Van Nieuwenhuysen, Ivan Gordon, and Jef Poortmans. Mechanical properties of sintered meso-porous silicon: a numerical model. *Nanoscale Research Letters*, 7(1):597, 2012.
- D. Bellet, P. Lamagnère, A. Vincent, and Y. Bréchet. Nanoindentation investigation of the Young's modulus of porous silicon. *Journal of Applied Physics*, 80(7):3772–3776, 1996.
- Hélène Magoaric and Alexandre Danescu. Modeling macroscopic elasticity of porous silicon. *Physica Status Solidi (C) Current Topics in Solid State Physics*, 6(7):1680–1684, 2009.
- Ch Populaire, Boudjema Remaki, Vladimir I. Lysenko, Daniel Barbier, H. Artmann, and Thierry Le Pannek. On mechanical properties of nanostructured meso-porous silicon. *Applied Physics Letters*, 83(7):1370–1372, 2003.
- Maurice Anthony Biot. Mechanics of deformation and acoustic propagation in porous media. *Journal of applied physics*, 33(4):1482–1498, 1962.
- H. J. McSkimin and P. Andreatch. Elastic moduli of silicon vs hydrostatic pressure at 25.0°C and - 195.8°C. *Journal of Applied Physics*, 35(7):2161–2165, 1964.
- Gaël Gautier. *Porous Silicon and Micro Fuel Cells*, pages 1–9. Springer International Publishing, Cham, 2017.
- John J. Hall. Electronic effects in the elastic constants of n-type silicon. *Phys. Rev.*, 161(1961):756–761, Sep 1967.
- Helmut Föll, M Christophersen, J Carstensen, and G Hasse. Formation and application of porous silicon. *Materials Science and Engineering: R: Reports*, 39(4):93–141, 2002.
- Gennadii Sergeevich Korotchenkov. *Porous silicon : from formation to application. Volume one. Formation and properties*. CRC Press, 2015.
- Amer Melhem, Domingos De Sousa Meneses, Caroline Andrezza-Vignolles, Thomas Defforge, Gael Gautier, and Nadjib Semmar. Structural, optical, and thermal analysis of n-type mesoporous silicon prepared by electrochemical etching. *The Journal of Physical Chemistry C*, 119(37):21443–21451, 2015.